



RESEARCH LETTER

10.1002/2018GL077525

Key Points:

- This is the first study of dust effects on atmospheric composition and density at high altitudes from 170 to 220 km using MAVEN
- Atmospheric densities including major and minor species increase strongly in response to dust increase in the lower atmosphere
- The observed density increases are due to hydrostatic expansion of the thermosphere and also involve other processes

Correspondence to:

G. Liu,
guiping@ssl.berkeley.edu

Citation:

Liu, G., England, S. L., Lillis, R. J., Withers, P., Mahaffy, P. R., Rowland, D. E., et al. (2018). Thermospheric expansion associated with dust increase in the lower atmosphere on Mars observed by MAVEN/NGIMS. *Geophysical Research Letters*, 45. <https://doi.org/10.1002/2018GL077525>

Received 8 FEB 2018

Accepted 14 MAR 2018

Accepted article online 23 MAR 2018

Thermospheric Expansion Associated With Dust Increase in the Lower Atmosphere on Mars Observed by MAVEN/NGIMS

Guiping Liu^{1,2} , Scott L. England³ , Robert J. Lillis¹ , Paul Withers^{4,5} , Paul R. Mahaffy⁶ , Douglas E. Rowland⁶ , Meredith Elrod⁶ , Mehdi Benna⁶ , David M. Kass⁷ , Diego Janches⁶ , and Bruce Jakosky⁸ 

¹Space Sciences Laboratory, University of California, Berkeley, CA, USA, ²CUA/GSFC, Greenbelt, MD, USA, ³Aerospace and Ocean Engineering, Virginia Polytechnic Institute and State University, Blacksburg, VA, USA, ⁴Department of Astronomy, Boston University, Boston, MA, USA, ⁵Center for Space Physics, Boston University, Boston, MA, USA, ⁶Goddard Space Flight Center, NASA, Greenbelt, MD, USA, ⁷Jet Propulsion Laboratory, California Institute of Technology, Pasadena, CA, USA, ⁸Laboratory for Atmosphere and Space Physics, University of Colorado Boulder, Boulder, CO, USA

Abstract We present for the first time the dramatic variations in atmospheric composition and density at high altitudes from 170 to 220 km in Mars' neutral thermosphere in response to dust increases in the lower atmosphere, observed by the in situ Neutral Gas Ion Mass Spectrometer onboard the Mars Atmosphere and Volatile EvolutioN satellite. The observations reveal that CO₂, Ar, N₂, CO, and O densities all increase up to ~200% compared to the longer-term running median densities. The density increases are seen throughout this altitude region, and the relative variations are seen to be stronger at higher altitudes. Density increases indicating the solar extreme ultraviolet influence are also seen. This study is consistent with that during increased dust load, the whole atmosphere expands and rises, and other processes may also be involved. The results agree with the general circulation model predictions, providing observational evidence for how dust increases affect different atmospheric species in the thermosphere.

1. Introduction

Dust increases in Mars' lower atmosphere are known to have significant impacts on the neutral upper atmosphere and thermosphere, being able to greatly increase atmospheric densities at ~100 to 160-km altitudes (e.g., Bell et al., 2007; Bougher et al., 2006; Keating et al., 1998; Withers & Pratt, 2013). Although dust is not lofted into these altitudes, the entire atmosphere expands due to aerosol heating, and as such, the rising of pressure levels from below dominates the density change at a given altitude (e.g., Bougher et al., 1997, 1999). Moreover, adiabatic heating/cooling associated with the modified atmospheric circulation could also affect the density and temperature change in the lower thermosphere (e.g., Bell et al., 2007; Bougher et al., 2006, 2009; González-Galindo et al., 2015; Withers & Pratt, 2013). In addition, changes in the altitude of the ionospheric peak in response to increased dust amounts have been observed (Keating et al., 1998; Withers, 2009).

Thermospheric density variations caused by dust have been reported using observations made via techniques including accelerometry (Bougher, Brain, et al., 2017; Keating et al., 1998), radio occultation (Bougher, Brain, et al., 2017; Withers & Pratt, 2013), and ultraviolet stellar occultation (Forget et al., 2009; Withers & Pratt, 2013). These observations have been limited to <160 km, that is, approximately the lower half of the thermosphere. From the aforementioned increases in the altitudes of isobaric levels during dust increases, we would expect increases in density of the upper remainder of the thermosphere and the "cold" component of the exosphere (i.e., the exponentially decreasing upward continuation of the thermosphere) at all altitudes above 160 km. However, densities derived from radio tracking at 370–430 km show no detectable increase corresponding with increased lower atmospheric dust load (Bruinsma et al., 2014), indicating that, at these higher altitudes, (a) some process is counteracting this pressure-level increase, (b) densities are dominated by a hot component produced nonthermally (e.g., sputtering; Luhmann et al., 1992) or photochemistry (e.g., Valeille et al., 2009), or a combination of both. The highest altitudes to which dust storm effects detectably penetrate are thus not known. In addition, if dusts impact the thermal structure of the atmosphere, they could potentially modify the distributions of atmospheric species at high altitudes, causing local

compositional changes. Continuous observations for thermospheric composition and density have become available since the operation of the Mars Atmosphere and Volatile Evolution (MAVEN) mission (Jakosky et al., 2015), which permit the investigation of such effects for the first time.

The variability of atmospheric temperature and density at the exobase has been simulated using general circulation models, taking into account the dust load variability (e.g., Bell et al., 2007; Bougher et al., 2006; González-Galindo et al., 2009, 2015; McDunn et al., 2010; Medvedev et al., 2013). The simulations exhibit large effects of increased dust on thermosphere dynamics and structure, and the strongest impacts are seen to occur coincident with the peak of the dust storm (González-Galindo et al., 2015). However, the model constraints are mostly based upon the aforementioned aerobraking accelerometer observations from Mars Global Surveyor, Mars Odyssey, Mars Reconnaissance Orbiter, and stellar occultation data from SPICAM. These observations cover the lower thermosphere part and limit the models' capability to predict the variations at higher altitudes.

For this study, we extend the altitude range of these analyses by utilizing in situ observations of atmospheric densities at ~170–220 km from the Neutral Gas and Ion Mass Spectrometer (NGIMS) (Mahaffy et al., 2014) onboard MAVEN during a sequence of dust increases in the lower atmosphere in 2017. These observations are for CO₂, Ar, N₂, CO, and O, which constitute both major and minor species of Mars' atmosphere, and allow for the study of dust effects on various species and the composition changes in the neutral thermosphere.

2. NGIMS Observations

Neutral Gas and Ion Mass Spectrometer is a quadrupole mass spectrometer, designed to measure atmospheric densities at altitudes below 500 km above the areoid (Mahaffy et al., 2014). The spacecraft is in an eccentric ~4.5-hr orbit, with apoapsis near 6,200 km. Periapsis is determined by an actively targeted density corridor of 0.05 to 0.15 kg/km³, usually occurring between 140 and 160 km (Jakosky et al., 2015). For each orbit, the number density of each atmospheric species is continuously measured throughout all altitudes, providing an altitude profile of density. These profiles have been used to study thermospheric compositional structure (Mahaffy et al., 2015), density changes associated with small- and large-scale atmospheric waves (e.g., England et al., 2016, 2017; Liu et al., 2017; Terada et al., 2017; Yiğit et al., 2015), to calculate photochemical escape rates of oxygen (Lillis et al., 2017), and also to characterize the seasonal and solar activity trends of temperatures and scale heights in the upper atmosphere and thermosphere (Bougher, Roeten, et al., 2017). Because the NGIMS noise floor is an absolute number of counts, the instrument is most sensitive at higher densities, hence lower altitudes, especially for the minor species. We have thus selected data below 220-km altitude for this study.

We have selected two time intervals, with interval 1 spanning 20 December 2016 to 30 May 2017 and interval 2 covering 1 August to 31 December 2015. Several events of dust increases in the lower atmosphere are observed during interval 1, and at interval 2, there are no large increases of dust (see Figure 1 and weather reports by NASA/JPL-Caltech at <http://www.msss.com>; Malin et al., 2017). Figure 1 shows the dust column opacity at 463 cm⁻¹ (22 μm) obtained by the infrared limb-staring radiometer (McCleese et al., 2007) onboard the Mars Climate Sounder (MCS). The standard MCS retrieval algorithm (Kleinböhl et al., 2009, 2011) produces profiles of dust extinction but not an explicit column opacity. In order to obtain a column opacity, a process very similar to Montabone et al. (2015) is used. If the profile reaches within 1¼ scale heights of the surface, it is extended to the surface by assuming the dust is well mixed. The dust profile is then integrated and normalized to 610 Pa to obtain a column opacity (reported at 463 cm⁻¹, 22 μm). In binning the column opacities, bins with 3 or fewer profiles were discarded (since the bin may be biased). All of the MCS data used are from the standard 2-D retrievals (Kleinböhl et al., 2017).

Over both time intervals, the NGIMS Level 2 version 7 revision 1 data are available for each day. As the observations are made over 4–5 orbits per day, the total numbers of density profiles available are more than 650 profiles during each interval for each species investigated.

Figure 2 shows the coverage of the NGIMS observations from 220-km periapsis altitudes along each orbit for each of the two selected time intervals. Each periapsis pass lasts for ~600 s, so the region measured during one orbit can cover ~20° latitude. The data span from ±70° latitude and cover a wide range of local times including daytime and nighttime hours. The latitude and local time spans are similar between the two

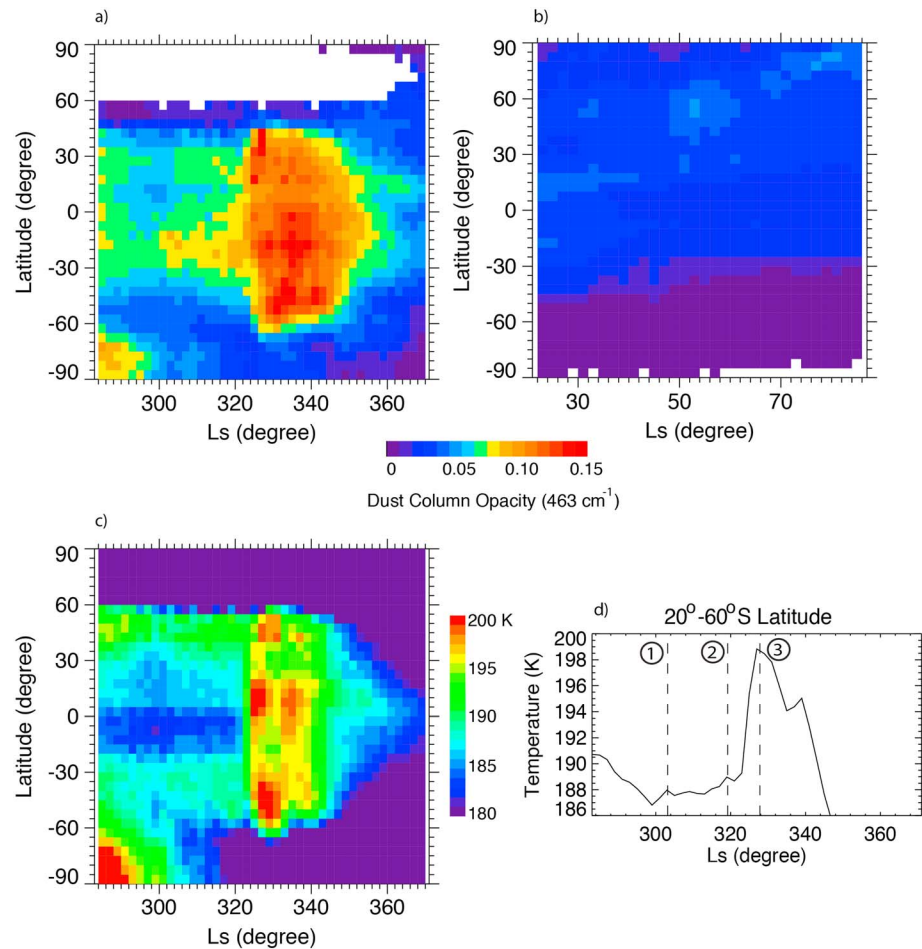


Figure 1. (a and b) Dust column opacity at 463 cm^{-1} ($22\text{ }\mu\text{m}$) from Mars Climate Sounder (MCS), presented at 2° Ls and 5° latitude bins during 20 December 2016 to 30 May 2017 and 1 August 1 to 31 December 2015. Dust increases over the latitude region from the equator to $\sim 20^\circ$ and 60°S around Ls of 303° , 320° , and 328° . (c and d) Atmospheric temperatures derived from the MCS measurements at 50 Pa ($\sim 25\text{ km}$ altitude). The line plot in (d) is for the averaged values between 20° and 60°S latitude, and the dashed lines mark the temperature peaks in response to the dust increase episodes.

time intervals, but they are in different dust storm seasons (e.g., Montabone et al., 2015; Shirley, 2014) ($L_s = \sim 280^\circ\text{--}360^\circ$ in the dust storm season for interval 1; $L_s = \sim 20^\circ\text{--}80^\circ$ in the nonstorm season for interval 2).

A few “deep dip” experiments have been carried out, targeting mass densities of $2.0\text{--}3.5\text{ kg/km}^3$ (Zurek et al., 2017), during which periapsis reaches as low as $\sim 120\text{ km}$ (see example for September of 2015 in Figure 2). These experiments allow for measurements approximately down to the homopause (i.e., the altitude below which turbulent mixing results in a uniform scale height for all species), and they are useful to characterize the entire upper atmosphere down to where it connects to the lower atmosphere (Jakosky et al., 2015). We have included the “deep dip” profiles during September of 2015 but for altitudes above 170 km, since the lowest altitudes are sampled very sparsely. As Figure 2 shows, profiles of all species analyzed always extend to at least 220 km; we have selected this altitude range from 170 to 220 km. The NGIMS observations are at high-altitude resolution (close to 1 km within the selected altitude range), so we have interpolated the data into regular grids at 1-km altitude steps.

Neutral Gas and Ion Mass Spectrometer has both open and closed source modes, which enable it to measure both nonreactive and reactive species. While the closed source is used to measure nonreactive species (CO_2 , Ar, and N_2), the open source measures both reactive and nonreactive species (CO and O). We have used five species, CO_2 , Ar, N_2 , CO, and O comprising all of the major constituents of Mars’ upper atmosphere. As the adsorption and subsequent separation of O by the walls of the instrument may impact the measurements

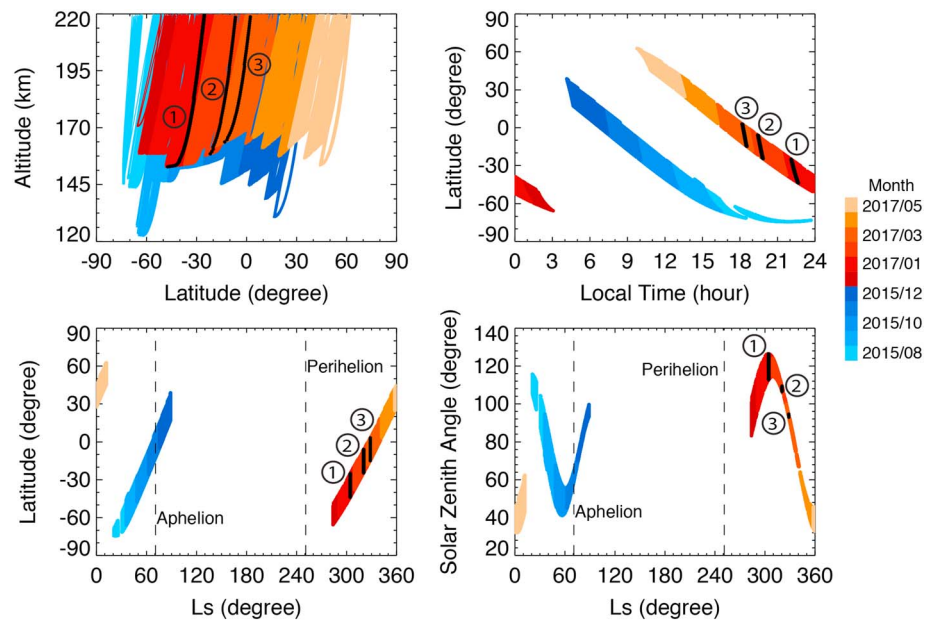


Figure 2. Distributions of the Neutral Gas and Ion Mass Spectrometer data below 220 km altitude (above the areoid) during two selected time intervals. The colors represent different months from both intervals 1 and 2, and the black strips highlight the data obtained during the maximum heating by increased dust. The data are presented versus latitude and altitude, local time and latitude, Ls (i.e., Mars season) and latitude, and Ls and solar zenith angle.

of O, CO, and CO₂ made after periapsis in each orbit (e.g., Mahaffy et al., 2014; Vuitton et al., 2008), we have only used the data in inbound portions.

3. Density Variations With Dust Increase

Figure 3a shows scatterplots of the measured Ar densities at altitudes from 170 to 220 km over interval 1 from 20 December 2016 to 30 May 2017, corresponding to the dust increase episodes. The latitudes of the data shift gradually from SH high latitudes to NH midlatitudes, and the local times change from midnight to daytime hours over the data shown in Figure 2. These density changes have been estimated for each altitude using the median densities of the 20° Ls (~40 days) running window. As the thermospheric response to a dust storm lasts about 20–120° Ls (Withers & Pratt, 2013), this window is sufficient to reduce the dust storm effects, the noise, short-term fluctuations, and variations associated with atmospheric tides. This running window also removes impacts due to short-term variations of solar rotation driven extreme ultraviolet (EUV) fluxes. Apparently, the calculated median densities vary smoothly with the changing latitudes and local times of the data. However, larger variations are seen, and there are many data points largely deviating from the calculated density patterns. During the dust increases (indicated by dashed lines), the Ar densities increase by a few times (above the 1-standard deviation level) and then drop quickly to lower levels within several degrees of Ls. The exact Ls (decay time scales) of these density peaks are not calculated as they are beyond the scope of this study. Nonetheless, coincide with dust increases, the densities are seen to increase, and these density increases are seen at all altitudes.

For interval 2, the Ar density (20° Ls running median) varies, following the change of latitude, season, and local time of the data. However, there are also density fluctuations present over this time interval in this non-storm season (see Figure 3b).

The density observations shown in Figure 3 are from individual orbits, and for the same days the observations are for different longitudes. The upper atmosphere is known to have an intrinsic orbit-to-orbit variability (Bougher et al., 2015; Bougher, Roeten, et al., 2017), and the NGIMS observations have revealed that the Ar density varies with longitude, having a longitudinal structure associated with atmospheric tides (e.g., England et al., 2016; Bougher, Brain, et al., 2017; Liu et al., 2017). To reduce this variability, the Ar densities observed for the

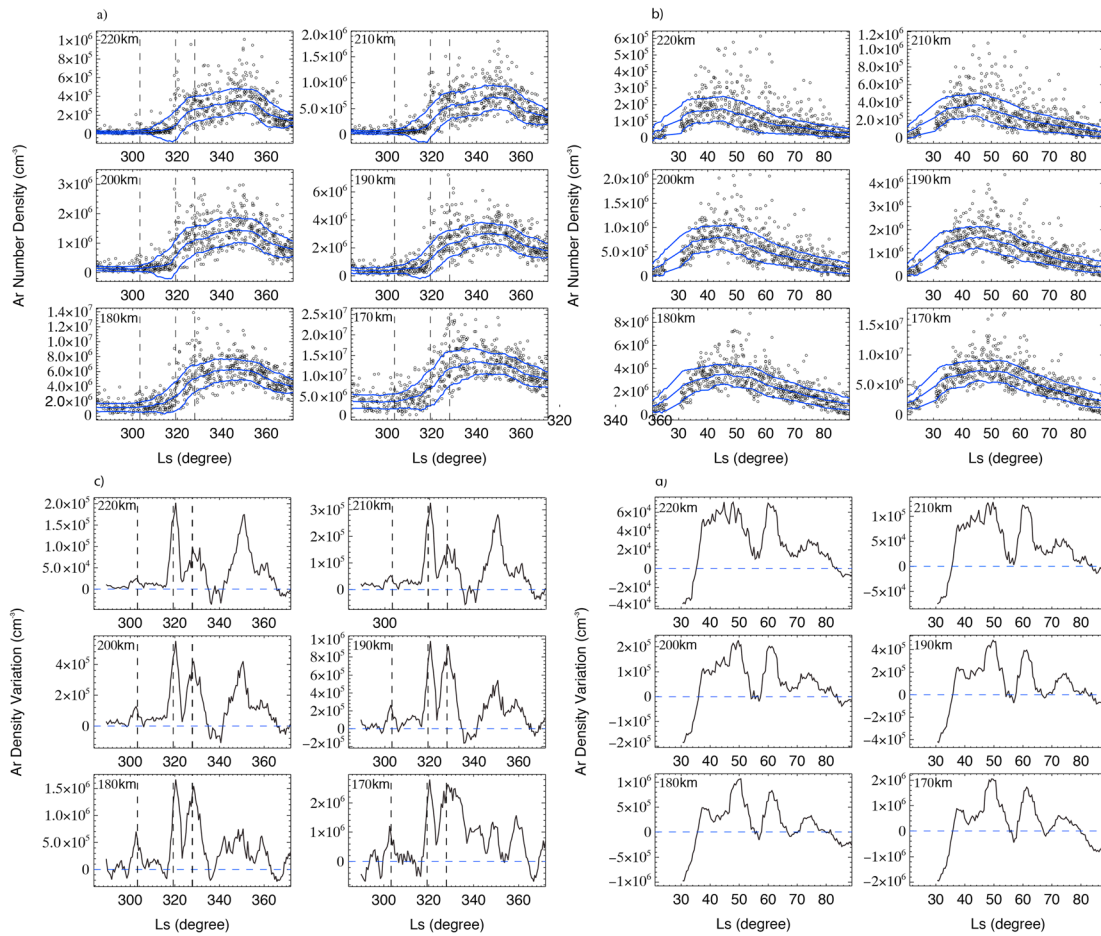


Figure 3. Ar densities at the given altitudes from 170 to 220 km, presented versus Ls for the time intervals of (a) 20 December 2016 to 30 May 2017 and (b) 1 August 1 to 31 December 2015. The blue curves are for the 20° Ls running medians, including the density changes with latitude and local time. The blue dashed curves represent the 1-standard deviations. The dashed black lines mark the peak heating of dust increases seen in the lower atmosphere. Ar density variations (differences of the observed densities with the calculated 20° Ls running median densities) are shown in (c) and (d) for the two time intervals. These variations have been smoothed using the 5° Ls running average.

same Ls are averaged. Figure 4 presents these averaged densities in comparison with the daily mean Lyman-Alpha irradiance, which is an indicator of the changing solar EUV heating in the thermosphere (Bougher, Roeten, et al., 2017). The density increases in response to dust increases are present, and there are also variations correspond with the EUV variations. The signatures are seen for Ls = ~340–360° and are seen to be clear in the vertical range between 190 and 220 km at higher altitudes. Similarly, the densities in the nonstorm interval have a solar rotation cadence (~13° Ls), indicating the solar influences.

The differences between the Ar densities and the calculated median densities are shown in Figure 3 at the given altitudes over the two time intervals. These differences have been smoothed through the 5° Ls (~10 days) running averaging to remove the noise. However, spikes of large density increases still present, coincident with the dust increases. Except these peaks, there are moderate density increases at a solar rotational cadence in the nonstorm season. These exhibit again the dramatic density variations in the thermosphere in response to dust and solar irradiance effects.

The Ar density variations appear to be the smallest for dust event 1, and the density increases are larger for events 2 and 3. Different density perturbations are observed in response to each of these dust increases. Given that each event has a unique feature such as the dust loading amount and its activity (e.g., Smith et al., 2006), the effects of individual dust increases are expected to be different. In addition, the densities are observed at nighttime for events 1 and 2 but during daytime hours for event 3 (see Figure 2). The day-night differences of the dust effects are also expected. For event 2, the largest Ar density increase is seen

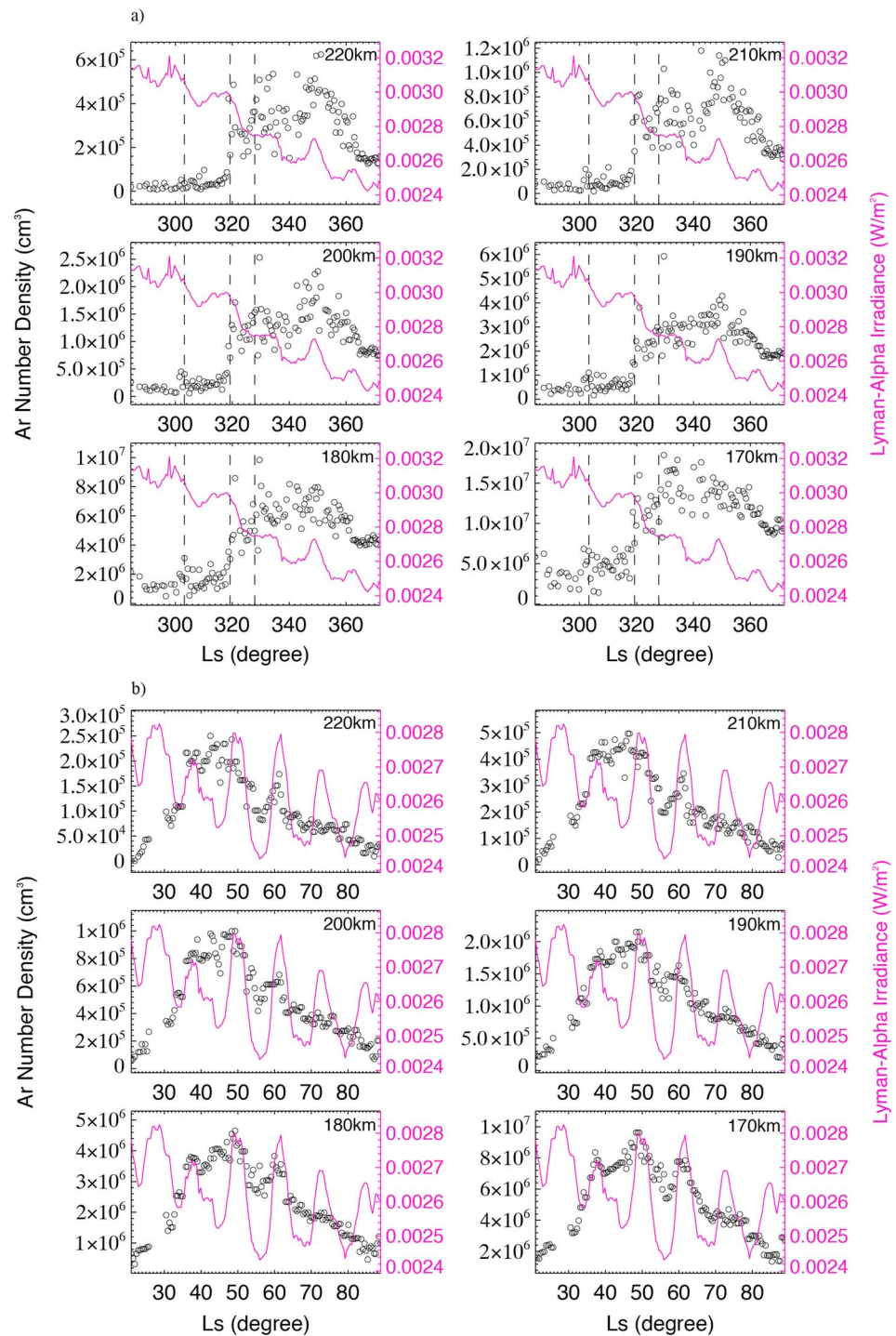


Figure 4. Averaged Ar densities for the same Ls and the daily mean Lyman-Alpha irradiance measured by the solar extreme ultraviolet monitor (Eparvier et al., 2015) on Mars Atmosphere and Volatile Evolution (in pink) during (a) 20 December 2016 to 30 May 2017 and (b) 1 August to 31 December 2015. The dashed black lines in (a) mark the peak heating of dust increases seen in the lower atmosphere.

to be $\sim 2 \times 10^5 \text{ cm}^{-3}$ at 220-km altitude, and the increase is about $5 \times 10^5 \text{ cm}^{-3}$ at 200-km altitude, and $\sim 1.5 \times 10^6 \text{ cm}^{-3}$ at 180-km altitude. Dust impacts are seen to be stronger at lower altitudes and for all events, which could be related to “larger” background densities at these altitudes as atmospheric densities increase exponentially with decreasing altitude. Furthermore, the density increases seen at $L_s = \sim 340\text{--}360^\circ$

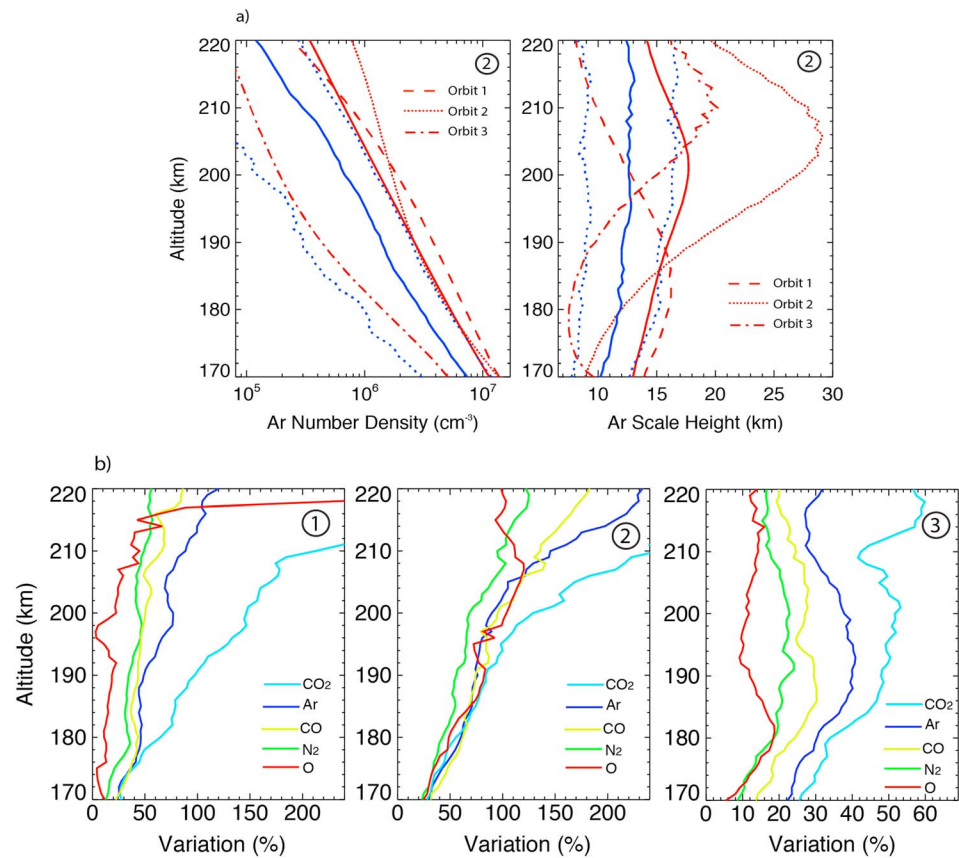


Figure 5. (a) Ar density and scale height profiles observed at dust increase event 2 ($\sim 320^\circ$ Ls) over three orbits shown in red. The solid red profiles are for the averaged values over the same Ls. Here for two orbits the densities are larger than the profiles shown in blue, and for orbit 3, the densities are smaller (the solid blue profiles are for the median values of the 20° Ls running windows, and the dot blue profiles denote one standard deviations of these values). (b) Relative density variations (normalized differences of the observed densities with the 20° Ls median densities) of CO_2 , Ar, CO, N_2 , and O observed during the same orbit passes in response to the three dust increase events in the lower atmosphere.

are smaller than the dust-driven variations (for events 2 and 3) specifically at 170 to 190-km altitudes but have larger values at higher altitudes, indicating the solar influences in the thermosphere.

Figure 5a shows the Ar densities, along with the derived scale heights, observed at dust event 2 (Ls $\sim 320^\circ$) for the selected vertical range. For comparison, the profiles calculated from the 20° Ls running windows, and the averages for the same Ls are also included. The observed densities and scale heights are shown for three orbital passes. Except for orbit 3, the densities are all larger than the values from the longer-term running windows.

As shown in the red dashed profile (orbit 1), the Ar density increases almost uniformly across the vertical range, by up to several times of the 20° Ls median values (blue solid profile). Being a nonreactive species, Ar acts as a passive tracer of vertical transport in the atmosphere. This density increase in this species implies that the atmosphere moves upward during the dust increase, as may be expected from the attendant warming of the lower atmosphere. This upward movement can be estimated using the altitude difference between the two profiles by selecting a constant density level. As shown, the movement is ~ 10 km uniformly throughout the investigated region. This ~ 10 -km movement upward is similar to the change in the height of the F1-ionospheric peak observed by MGS during the Noachis regional dust storm (Keating et al., 1998). Correspondingly, the red dashed and blue solid profiles of scale height show that the scale heights are between 10 and 15 km, and they (and hence temperatures) have smaller changes (relative to orbit 2). Previous studies have suggested that during dust storms, the whole atmosphere shifts upward (e.g., Bougher et al., 1997, 1999; Withers & Pratt, 2013). The rising atmospheric layer increases the density at a given altitude, so the suggestion is consistent with the variations seen in this study.

In contrast, the other profile (red dot for orbit 2) has larger variations specifically at 190 to 220-km altitudes. The density increases are stronger, and the corresponding scale heights also increase largely (up to factor of 2) at these altitudes. Given that scale height is proportional to temperature, the pronounced increase in scale height implies that the temperature rises significantly. To account for these large variations, other processes such as adiabatic heating/cooling associated with the modified atmospheric circulation (e.g., Bell et al., 2007; Bougher et al., 2006, 2009; González-Galindo et al., 2015; Withers & Pratt, 2013) should also be considered. In addition, the longitudinal differences sampled by these orbits may also play a role.

Figure 5b shows the relative density variations (normalized differences of the observed densities with the 20° Ls median densities) for atmospheric species of CO₂, Ar, CO, N₂, and O at 170 to 220-km altitude over each of the dust increase events. The density in each species is seen to increase throughout this vertical column, and the density increases are seen to be stronger at higher altitudes. Moreover, the density variations are dependent on species: CO₂ has the largest density changes, and the changes in other species are smaller. This is reasonable as CO₂ has the smallest scale height in the thermosphere.

Atmospheric density increases associated with dust increases are observed in this study in the altitude range from 170 to 220 km. This is not surprising as, during dust storms, the whole atmosphere expands and rises, increasing the densities in the intervening altitudes (e.g., Bougher et al., 1997, 1999; Withers & Pratt, 2013). Previous studies have reported the density increases observed at altitudes as high as 160 km (Withers & Pratt, 2013). The present study is for higher altitudes, showing that the dust influences reach ~220-km altitude in the thermosphere.

No density increases have been detected at 370 to 430-km altitudes in response to increased dust levels in the lower atmosphere (Bruinsma et al., 2014), implying that dust might not generally affect the exosphere. At these higher altitudes, there should be a “cooling” process, counteracting the atmosphere warming and the pressure level and density increase. The lower exosphere is a transition region for which fluid processes and kinetic processes compete to influence neutral species distributions. Thus, new physical processes come into play above the thermosphere affecting densities (and temperatures), for which global redistribution (and cooling) may occur. This study observes the dust storm effects at 170 to 220-km altitudes, and the effects are seen to be stronger at higher altitudes. However, the altitude limits where these effects dissipate have not been examined.

Many general circulation models have been used to study the variations in the upper atmosphere and thermosphere at varying atmospheric dust load conditions (e.g., Bell et al., 2007; Bougher et al., 2006; González-Galindo et al., 2009, 2015; Medvedev et al., 2013). These models have simulated large increases in thermospheric density and temperature corresponding to dust storms. Comparing between the lowest and highest dust mixing heights, the neutral densities near the equator are seen to increase by the factor of 2 at 120-km altitude (Bell et al., 2007). Although no comparisons have been performed for the same dust increase events, results of this study are in general consistent with the model predictions.

4. Summary

Using in situ measurements by MAVEN/NGIMS, we have performed the first observational study of the effects of increased dust in the lower atmosphere on atmospheric composition and density at altitudes from 170 to 220 km in Mars' thermosphere. Heretofore, density increases associated with dust increases have been observed at altitudes as high as 160 km and are not observed at 370–430 km in the exosphere.

For this study, we have analyzed the density variations for atmospheric species of CO₂, Ar, CO, N₂, and O, the primary species in Mars' atmosphere. We have compared the variations between two time intervals with overlapping latitudes and local times but different Ls. The key results are summarized as follows:

1. The Ar observations during January to April 2017 reveal large density increases coincident with the peak temperature enhancements associated with the dust increases in the lower atmosphere. Compared to the longer-term running median density changes, the density increases are up to 200% at 220-km altitude and less than 50% at 170-km altitude. The variations are seen at all altitudes throughout 170–220 km but are seen to be stronger at higher altitudes that may correspond to higher temperatures.
2. At dust increase event 2, the thermosphere is observed to move upward by ~10-km altitude, and scale height is almost the same throughout the altitude column investigated. However, for some orbits, the

vertical movements and scale height changes are seen to be larger at 190 to 220-km altitudes. These indicate that during dust increases the whole atmosphere expands and rises, and other processes such as the modified circulation may also be involved.

3. The large density increases at dust increases are seen for all species of CO₂, Ar, CO, N₂, and O throughout the altitude region from 170 to 220 km. CO₂ has the largest density increases, and the increases in other species are smaller. These show that the density variations associated are dependent on atmospheric species.

Acknowledgments

The NGIMS Level 2 version 7 and EUV Level 3 version 10 data are publicly available on the Planetary Data System (PDS) at <http://pds.nasa.gov> as well as the MAVEN Science Data Center (SDC) at LASP. The MCS analyses use retrievals v5.2, which are available in the PDS. G.L., S.L.E., and R.J. Lillis were supported through NASA grant NNX16AJ42G. The MAVEN mission has been funded through the NASA Mars Exploration Program. D.M.K.'s contribution was performed at the Jet Propulsion Laboratory, California Institute of Technology, under contract with NASA. Government sponsorship is acknowledged.

References

- Bell, J. M., Bougher, S. W., & Murphy, J. R. (2007). Vertical dust mixing and the interannual variations in the Mars thermosphere. *Journal of Geophysical Research*, *112*, E12002. <https://doi.org/10.1029/2006JE002856>
- Bougher, S. W., Bell, J. M., Murphy, J. R., Lopez-Valverde, M. A., & Withers, P. G. (2006). Polar warming in the Mars thermosphere: Seasonal variations owing to changing isolation and dust distributions. *Geophysical Research Letters*, *33*, L02203. <https://doi.org/10.1029/2005GL024059>
- Bougher, S. W., Brain, D. A., Fox, J. L., Gonzalez-Galindo, F., Simon-Wedlund, C., & Withers, P. G. (2017). Chapter 14: Upper neutral atmosphere and ionosphere. In B. Haberle, et al. (Eds.), *The atmosphere and climate of Mars* (pp. 433–463). Cambridge University Press. <https://doi.org/10.1017/9781107016187>
- Bougher, S. W., McDunn, T. M., Zoldak, K. A., & Forbes, J. M. (2009). Solar cycle variability of Mars dayside exospheric temperatures: Model evaluation of underlying thermal balances. *Geophysical Research Letters*, *36*, L05201. <https://doi.org/10.1029/2008GL036376>
- Bougher, S. W., Murphy, J., & Haberle, R. M. (1997). Dust storm impacts on the Mars upper atmosphere. *Advances in Space Research*, *19*(8), 1255–1260. [https://doi.org/10.1016/S0273-1177\(97\)00278-0](https://doi.org/10.1016/S0273-1177(97)00278-0)
- Bougher, S. W., Roeten, K. J., Olsen, K., Mahaffy, P. R., Benna, M., Elrod, M., et al. (2017). The structure and variability of Mars dayside thermosphere from MAVEN NGIMS and IUVS measurements in scale heights and temperatures. *Journal of Geophysical Research: Space Physics*, *122*, 1296–1313. <https://doi.org/10.1002/2016JA023454>
- Bougher, S., Keating, G., Zurek, R., Murphy, J., Haberle, R., Hollingsworth, J., & Clancy, R. T. (1999). Mars Global Surveyor aerobraking: Atmospheric trends and model interpretation. *Advances in Space Research*, *23*(11), 1887–1897. [https://doi.org/10.1016/S0273-1177\(99\)00272-0](https://doi.org/10.1016/S0273-1177(99)00272-0)
- Bougher, S., Jakosky, B., Halekas, J., Grebowsky, J., Luhmann, J., Mahaffy, P., et al. (2015). Early MAVEN deep dip campaign reveals thermosphere and ionosphere variability. *Science*, *350*(6261), aad0459. <https://doi.org/10.1126/science.aad0459>
- Bruinsma, S., Forbes, J. M., Marty, J.-C., Zhang, X., & Smith, M. D. (2014). Long-term variability of Mars' exosphere based on precise orbital analysis of Mars Global Surveyor and Mars Odyssey. *Journal of Geophysical Research: Planets*, *119*, 210–218. <https://doi.org/10.1002/2013JE004491>
- England, S. L., Liu, G., Withers, P., Yiğit, E., Lo, D., Jain, S., et al. (2016). Simultaneous observations of atmospheric tides from combined in situ and remote observations at Mars from the MAVEN spacecraft. *Journal of Geophysical Research: Planets*, *121*, 594–607. <https://doi.org/10.1002/2016JE004997>
- England, S. L., Liu, G., Yiğit, E., Mahaffy, P. R., Elrod, M., Benna, M., et al. (2017). MAVEN NGIMS observations of atmospheric gravity waves in the Martian thermosphere. *Journal of Geophysical Research: Space Physics*, *122*, 2310–2335. <https://doi.org/10.1002/2016JA023475>
- Eparvier, F. G., Chamberlin, P. C., Woods, T. N., & Thiemann, E. M. B. (2015). The solar extreme ultraviolet monitor for MAVEN. *Space Science Reviews*, *195*(1–4), 293–301. <https://doi.org/10.1007/s11214-015-0195-2>
- Forget, F., Montmessin, F., Bertaux, J.-L., González-Galindo, F., Lebonhols, S., Quémerals, E., et al. (2009). Density and temperatures of the upper atmosphere measured by stellar occultations with Mars Express SPICAM. *Journal of Geophysical Research*, *114*, E01004. <https://doi.org/10.1029/2008JE003086>
- González-Galindo, F., Forget, F., López-Valverde, M. A., Angelats i Coll, M., & Millour, E. (2009). A ground-to-exosphere Martian general circulation model: 1. Seasonal, diurnal, and solar cycle variation of thermospheric temperatures. *Journal of Geophysical Research*, *114*, E04001. <https://doi.org/10.1029/2008JE003246>
- González-Galindo, F., López-Valverde, M. A., Forget, F., García-Comas, M., Millour, E., & Montabone, L. (2015). Variability of the Martian thermosphere during eight Martian years as simulated by a ground-to-exosphere global circulation model. *Journal of Geophysical Research: Planets*, *120*, 2020–2035. <https://doi.org/10.1002/2015JE004925>
- Jakosky, B. M., Lin, R. P., Grebowsky, J. M., Luhmann, J. G., Mitchell, D. F., Beutelschies, G., et al. (2015). The Mars Atmosphere and Volatile Evolution (MAVEN) mission. *Space Science Reviews*, *195*(1–4), 3–48. <https://doi.org/10.1007/s11214-015-0139-x>
- Keating, G. M., Bougher, S. W., Zurek, R. W., Tolson, R. H., Cancro, G. J., Noll, S. N., et al. (1998). The structure of the upper atmosphere of Mars: In situ accelerometer measurements from Mars Global Surveyor. *Science*, *279*(5357), 1672–1676. <https://doi.org/10.1126/science.279.5357.1672>
- Kleinböhl, A., Friedson, A. J., & Schofield, J. T. (2017). Two-dimensional radiative transfer for the retrieval of limb emission measurements in the Martian atmosphere. *Journal of Quantitative Spectroscopy and Radiation Transfer*, *187*, 511–522. <https://doi.org/10.1016/j.jqsrt.2016.07.009>
- Kleinböhl, A., Schofield, J. T., Abdou, W. A., Irwin, P. J., & de Kok, R. (2011). A single-scattering approximation for infrared radiative transfer in limb geometry in the Martian atmosphere. *Journal of Quantitative Spectroscopy and Radiation Transfer*, *112*(10), 1568–1580. <https://doi.org/10.1016/j.jqsrt.2011.03.006>
- Kleinböhl, A., Schofield, J. T., Kass, D. M., Abdou, W. A., Backus, C. R., Sen, B., et al. (2009). Mars Climate Sounder limb profile retrieval of atmospheric temperature, pressure, dust and water ice opacity. *Journal of Geophysical Research*, *114*, E10006. <https://doi.org/10.1029/2009JE003358>
- Lillis, R. J., Deighan, J., Fox, J. L., Bougher, S. W., Lee, Y., Combi, M. R., et al. (2017). Photochemical escape of oxygen from Mars: First results from MAVEN in situ data. *Journal of Geophysical Research: Space Physics*, *122*, 3815–3836. <https://doi.org/10.1002/2016JA023525>
- Liu, G., England, S., Lillis, R. J., Mahaffy, P. R., Elrod, M., Benna, M., & Jakosky, B. (2017). Longitudinal structures in Mars' upper atmosphere as observed by MAVEN/NGIMS. *Journal of Geophysical Research: Space Physics*, *122*, 1258–1268. <https://doi.org/10.1002/2016JA023455>
- Luhmann, J. G., Johnson, R. E., & Zhang, M. H. G. (1992). Evolutionary impact of sputtering of the Martian atmosphere by O⁺ pick up ions. *Geophysical Research Letters*, *19*(21), 2151–2154. <https://doi.org/10.1029/92GL02485>

- Mahaffy, P. R., Benna, M., Elrod, M., Yelle, R. V., Bougher, S. W., Stone, S. W., & Jakosky, B. M. (2015). Structure and composition of the neutral upper atmosphere of Mars from the MAVEN NGIMS investigation. *Geophysical Research Letters*, *42*, 8951–8957. <https://doi.org/10.1002/2015GL065329>
- Mahaffy, P. R., Richard Hodges, R., Benna, M., King, T., Arvey, R., Barciniak, M., et al. (2014). The Neutral Gas and Ion Mass Spectrometer on the Mars Atmosphere and Volatile Evolution mission. *Space Science Reviews*, *185*(1–4), 27–61. <https://doi.org/10.1007/s11214-11014-10091-11211>
- Malin, M. C., Cantor, B. A., & Britton, A. W. (2017). MRO MARCI weather report, Malin Space Science Systems Captioned Image Release, MSSS.
- McCleese, D. J., Schofield, J. T., Taylor, F. W., Calcutt, S. B., Foote, M. C., Kass, D. M., et al. (2007). Mars Climate Sounder: An investigation of thermal and water vapor structure, dust and condensate distributions in the atmosphere, and energy balance of the polar regions. *Journal of Geophysical Research*, *112*, E050506. <https://doi.org/10.1029/2006JE002790>
- McDunn, T. L., Bougher, S. W., Murphy, J., Smith, M. D., Forget, F., Bertaux, J.-L., & Montmessin, F. (2010). Simulating the density and thermal structure of the middle atmosphere (80–130 km) of Mars using the MGCM-MTGCM: A comparison with MEX/SPICAM observations. *Icarus*, *206*(1), 5–17. <https://doi.org/10.1016/j.icarus.2009/06.034>
- Medvedev, A. S., Yiğit, E., Kuroda, T., & Hartogh, P. (2013). General circulation modeling of the Martian upper atmosphere during global dust storms. *Journal of Geophysical Research: Planets*, *118*, 2234–2246. <https://doi.org/10.1002/2013JE004429>
- Montabone, L., Forget, F., Millour, E., Wilson, R., Lewis, S., Cantor, B., et al. (2015). Eight-year climatology of dust optical depth on Mars. *Icarus*, *251*, 65–95. <https://doi.org/10.1016/j.icarus.2014.12.034>
- Shirley, J. H. (2014). Solar system dynamics and global-scale dust storms on Mars. *Icarus*, *245*, 282–294. <https://doi.org/10.1016/j.icarus.2014.08.038>
- Smith, M. D., Wolff, M. J., Spanovich, N., Ghosh, A., Banfield, D., Christensen, P. R., et al. (2006). One Martian year of atmospheric observations using MER mini-TES. *Journal of Geophysical Research*, *111*, E12S13. <https://doi.org/10.1029/2006JE002770>
- Terada, N., Leblanc, F., Nakagawa, H., Medvedev, A. S., Yiğit, E., Kuroda, T., et al. (2017). Global distribution and parameter dependences of gravity wave activity in the Martian upper atmosphere derived from MAVEN/NGIMS observations. *Journal of Geophysical Research: Space Physics*, *122*, 2374–2397. <https://doi.org/10.1002/2016JA023476>
- Vailleille, A., Combi, M. R., Bougher, S. W., Tenishev, V., & Nagy, A. F. (2009). Three-dimensional study of Mars upper thermosphere/ionosphere and hot oxygen corona: 2. Solar-cycle, seasonal variations, and evolution over history. *Journal of Geophysical Research*, *114*, E11006. <https://doi.org/10.1029/2009JE003389>
- Vuitton, V., Yelle, R. V., & Cui, J. (2008). Formation and distribution of benzene on Titan. *Journal of Geophysical Research*, *113*, E05007. <https://doi.org/10.1029/2007JE002997>
- Withers, P. (2009). A review of observed variability in the dayside ionosphere of Mars. *Advances in Space Research*, *44*(3), 277–307. <https://doi.org/10.1016/j.asr.2009.04.027>
- Withers, P., & Pratt, R. (2013). An observational study of the response of the upper atmosphere of Mars to lower atmospheric dust storms. *Icarus*, *225*(1), 378–389. <https://doi.org/10.1016/j.icarus.2013.02.032>
- Yiğit, E., England, S. L., Liu, G., Medvedev, A. S., Mahaffy, P. R., Kuroda, T., & Jakosky, B. M. (2015). High-altitude gravity waves in the Martian thermosphere observed by MAVEN/NGIMS and modeled by a gravity wave scheme. *Geophysical Research Letters*, *42*, 8993–9000. <https://doi.org/10.1002/2015GL065307>
- Zurek, R. W., Tolson, R. A., Bougher, S. W., Lugo, R. A., Baird, D. T., Bell, J. M., & Jakosky, B. M. (2017). Mars thermosphere as seen in MAVEN accelerometer data. *Journal of Geophysical Research: Space Physics*, *122*, 3798–3814. <https://doi.org/10.1002/2016JA023641>